INTERNATIONAL JOURNAL OF NOVEL RESEARCH AND DEVELOPMENT (IJNRD)
© 2026 IJNRD | Volume 11, Issue 1, January 2026 | ISSN: 2456-4184 | IJNRD.ORG

DEGRADATION OF ORGANIC POLLUTANTS BY $BaPbCe_2O_7$ NANO-PHOTOCATALYST: BENIGN WATER TREATMENT

Tejveer Singh Tanwer, Jinesh Menaria, Dushyant Kumar Prajapati, Jeevan Kunwar Chouhan and Shipra Bhardwaj

[1,2,3,4]Research Scholar, Department of Chemistry, Government Meera Girls College, Mohan Lal Sukhadia University, Udaipur, Rajasthan-313001, India.

[5]Professor, Department of Chemistry, Government Meera Girls College, Mohan Lal Sukhadia University, Udaipur, Rajasthan-313001, India.

Abstract: A novel $BaPbCe_2O_7$ nano-photocatalyst was synthesized through a controlled co-precipitation route followed by calcination, resulting in a product yield of 73% and was characterized using various analytical techniques. UV–Vis spectroscopy revealed an optical band gap of 2.32 eV. The resulting nanoparticles (NPs) were subsequently evaluated for their photocatalytic efficiency in degrading the dyes Azure A (AA), Toluidine blue (TB), and Erythrosine B (EB). A detailed kinetic study was performed to identify the optimal parameters for photocatalytic activity. The nano-photocatalyst exhibited remarkable performance, achieving degradation efficiencies of 87% for AA, 98% for TB and 79% for EB within just 40, 18 and 70 minutes of irradiation respectively. Radical scavenging experiments confirmed the participation of free radical reactive species in the degradation pathways. In addition, recyclability assessments demonstrated that the catalyst maintained nearly consistent activity over five successive cycles, indicating its stability and reusability. A plausible mechanism describing the photocatalytic degradation process has also been proposed.

IndexTerms: Photocatalysis, Photodegradation, Coprecipitation, Dye degradation, Water treatment.

1. Introduction

Azure A is defined as a basic dye belonging to the thiazine series, characterized by its violet blue color. It is prepared by oxidizing methylene blue with potassium dichromate and is used for staining purposes, notably in nuclear staining and demonstrating aldehyde reactions in tissues [1]. Toluidine blue (also known as tolonium chloride) is an acidophilic metachromatic dye that selectively stains acidic tissue components (sulfates, carboxylates, and phosphate radicals) [2]. Toluidine blue (TB) has an affinity for nucleic acids and therefore binds to nuclear material of tissues with a high DNA and RNA content [3]. It is a member of the thiazine group and is partially soluble in both water and alcohol [4]. Erythrosine B (EB) is an important xanthene dye and is extensively used as a coloring variety of foods like sweets, creams, ice cream, cake, in cosmetic and pharmaceutical industry, pills coverage, syrups, toothpaste, make up products, bath and shower products, hair-care products etc. It is used in most of the countries despite its toxic and carcinogenic effects against animals and humans [5].

Photocatalysis has emerged as a promising technology for environmental remediation and sustainable energy applications, in which photocatalysts utilize light energy to initiate and drive chemical reactions. Upon light irradiation, electrons are excited from the valence band to the conduction band, generating electron–hole pairs that participate in oxidation and reduction processes [6, 7]. The photocatalytic performance is influenced by several key parameters, including band gap energy, light intensity, catalyst dosage, solution pH, reactant concentration etc. [8]. Photocatalysts can be broadly classified into various categories such as conventional metal oxides (e.g. TiO_2 and ZnO), metal sulfides, graphene-based materials, and plasmonic photocatalysts, each possessing distinct properties and application potentials [9, 10].

BaO nanoparticles (BaO NPs) possess distinctive properties such as a highly reactive surface, wide band gap, excellent oxygen adsorption capacity, wide availability, cost-effectiveness, narrow emission, and strong electrical conductivity, enabling their applications in crown glass manufacturing, humidity sensing, and photocatalysis, as well as in medical and pharmaceutical fields including diagnostic imaging, orthopedic treatments, and in-vitro studies of apoptosis and DNA damage [11–14]. Lead oxide nanoparticles (PbO NPs) exhibit promising photocatalytic activity owing to their favorable band gap and efficient light absorption capability and is an important industrial material widely used in batteries, composite electrodes, optical sensors, reusable catalysts, and the glass industry [15, 16]. Cerium oxide (CeO_2) is another well-known semiconductor photocatalyst with diverse applications. Its band gap typically ranges from 2.6 to 3.4 eV, depending on the synthesis method [17, 18]. The photocatalytic and photoelectrode performance of CeO_2 arises from its high band gap energy, elevated refractive index, optical transparency in the visible region, excellent oxygen storage capacity, and high chemical reactivity, making it suitable for the degradation of various pollutants [19, 20]. When exposed to light irradiation, these nanoparticles can effectively initiate and promote degradation reactions, offering a sustainable and energy-efficient approach for wastewater treatment. Considering the synergistic advantages of multicomponent photocatalysts and their crucial role in advanced oxidation processes (AOPs), the present work reports the photocatalytic application of a novel quaternary photocatalyst, $BaPbCe_2O_7$, for efficient dye removal from wastewater systems. The synthesis, comprehensive characterization of $BaPbCe_2O_7$ nano-particles, in terms of crystallinity, morphology, phase purity, elemental composition, and optical properties using a range of spectroscopic and analytical techniques was carried out [21]. Prepared photocatalyst was then used further for removal of various dyes considering them as role model of their corresponding groups. Scavenger study helped to rule out the degradation mechanism and reuse of the material endorsed its stability and efficacy. The details are presented here by.

II. Experimental

2.1 Materials and Method

Barium nitrate, lead nitrate and cerous nitrate (Merck) were used as precursor materials for the synthesis of the photocatalyst, while sodium hydroxide (CDH) served as the precipitating agent. The pH of the reaction solutions was adjusted using hydrochloric acid and sodium hydroxide (both from CDH) and monitored with a pen-type pH meter (Hena, imported). UV–Vis spectrophotometry (CHINO) was employed for kinetic studies by recording the optical density of the solutions at predetermined time intervals. Photocatalytic irradiation was carried out using a 200W tungsten lamp (Philips) and the light intensity was measured with a solarimeter (New CHEM DT-1307). Reactive species trapping experiments were conducted using scavengers such as isopropanol, EDTA, KI and ammonium oxalate. All chemicals used were of laboratory reagent (LR) grade, with purities ranging from approximately 95% to 99%.

2.2 Instrumentation:

The synthesized $BaPbCe_2O_7$ photocatalyst was comprehensively characterized for crystal size by X-ray diffraction (XRD), field-emission scanning electron microscopy (FE-SEM) was done for morphology, elemental composition was analyzed using energy-dispersive X-ray spectroscopy (EDS) attached to the SEM. X-ray photoelectron spectroscopy (XPS) measurements were carried out to investigate the surface chemical states and elemental composition. UV–Vis diffuse reflectance spectra (DRS) were obtained using a UV–Vis–NIR spectrophotometer to study the optical properties of the photocatalyst. High-resolution transmission electron microscopy (HRTEM) analysis was performed to examine particle size and lattice features [21].

The photocatalytic degradation of the dye was monitored by measuring the absorbance at characteristic wavelengths using a UV–Vis spectrophotometer (CHINO). The degradation efficiency was calculated using the following equation:

$$\%\text{Degradation} = (C_0 - C)/C_0 \times 100$$

where C_0 and C represent the initial dye concentration and the concentration at a given irradiation time, respectively.

III. Results and Discussion

3.1 Synthesis and Characterization of $BaPbCe_2O_7$ nanoparticles:

$BaPbCe_2O_7$ nanomaterial was synthesized using a solid co-precipitation method under carefully controlled experimental conditions corresponding to a yield yellow solid of 91.8%. It was subsequently calcined at 500 °C for 2 h. After calcination, the material turned black, yielding 33.23 g of the final product, which corresponds to an overall yield of 73%.

The EDS spectrum of the synthesized $BaPbCe_2O_7$ nanoparticles confirmed the successful formation of the quaternary oxide, as the presence of Ba, Pb, Ce, and O was detected with elemental weight percentages of 13.73%, 20.72%, 26.62% and 11.20% respectively. X-ray diffraction (XRD) analysis demonstrated the nanocrystalline nature of the material, with an average crystallite size of 58.12 nm. X-ray photoelectron spectroscopy (XPS) analysis revealed characteristic peaks indicating the coexistence of Ba in +2, Pb in +2 and cerium in mixed oxidation states (Ce^{3+}/Ce^{4+}). UV–Vis spectroscopic analysis further indicated an optical band gap energy of 2.32 eV, confirming the visible-light-responsive nature of the synthesized photocatalyst [21].

3.2 Photocatalytic activity of $BaPbCe_2O_7$ nanoparticles:

Kinetic studies were performed by adding the photocatalyst to an aqueous dye solution in a borosilicate beaker, adjusting the pH, and exposing the mixture to light irradiation. The optical density (O.D.) was recorded at regular time intervals. A linear relationship between 1+log O.D. and irradiation time was observed (figure 1), indicating consistent reaction kinetics. Various models, including pseudo-first-order and pseudo-second-order (Type-1, Type-2, Type-3, Type-4, and Type-5), are studied to understand the degradation process. After analyzing the data, it is observed that the pseudo-first-order model best explained the degradation process. The optimized conditions for the breakdown of dyes are identified as follows:

Azure A (AA): pH 10.0, photocatalyst 0.12 g, dye concentration 0.4×10^{-4} M and light intensity 1960 $mWcm^{-2}$ Toluidine blue (TB): pH 9.1, photocatalyst 0.16 g, dye concentration 1.0×10^{-5} M and light intensity 1960 $mWcm^{-2}$ Erythrosine B (EB): pH 10.0, photocatalyst 0.16 g, dye concentration 4.8×10^{-3} M and light intensity 1710 $mWcm^{-2}$ Careful control of these factors is crucial for the z effective removal of dyes. A typical run for each dye is given in figure 1(a) (b) (c).

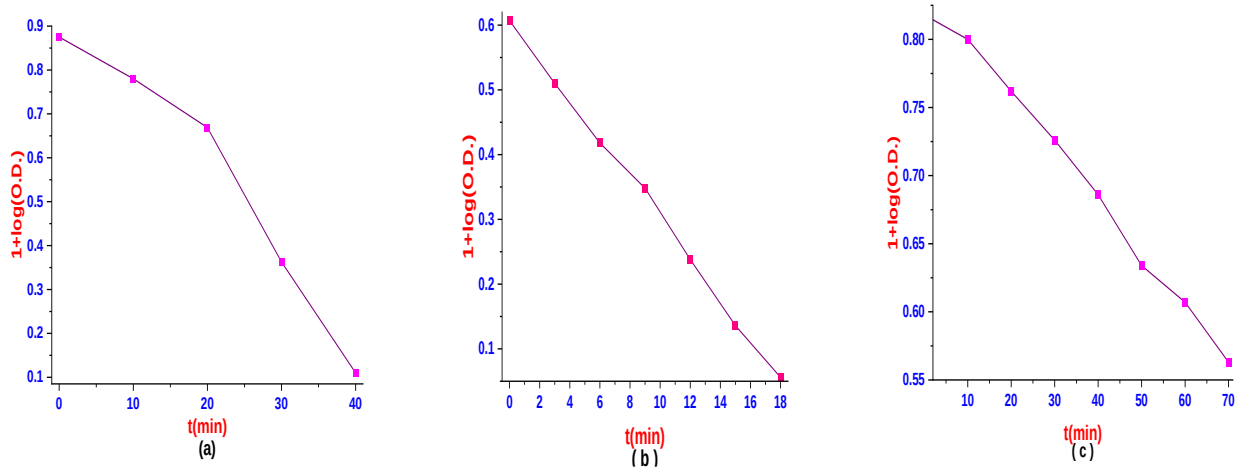

Figure 1: A typical run (a) AA (b) TB (c) EB

3.3 Effect of $BaPbCe_2O_7$ photocatalyst doses:

The effect of $BaPbCe_2O_7$ photocatalyst dosage on the degradation efficiency was systematically examined by varying the catalyst amount while keeping all other experimental parameters constant. The results, depicted in figure 2, indicate that the maximum degradation rates for AA, TB, and EB dyes were achieved at photocatalyst dosages of 0.12 g, 0.16 g and 0.16 g, respectively. The corresponding rate constants are summarized in table 1. The observed enhancement in degradation efficiency at optimal catalyst loading can be attributed to the increased number of active surface sites and improved light absorption, which facilitate the generation

of a greater number of electron–hole pairs. However, a further increase in photocatalyst dosage resulted in a decline in the reaction rate. This decrease is likely due to generation of greater number of electron–hole pairs causing their recombination and light scattering effects at higher catalyst concentrations, which collectively suppress the overall photocatalytic performance.

Table 1: Rate constants at different doses of $BaPbCe_2O_7$ photocatalyst

Doses of $BaPbCe_2O_7$ photocatalyst (g/50mL)	AA Rate constant × 10^{-4} (Sec^{-1})	TB Rate constant × 10^{-4} (Sec^{-1})	EB Rate constant × 10^{-4} (Sec^{-1})
0.02	-----	-----	1.36
0.04	-----	5.40	1.18
0.06	5.48	7.50	1.39
0.08	4.90	9.28	1.32
0.10	3.79	6.64	0.94
0.12	**5.96**	9.95	0.95
0.14	5.86	10.57	0.91
0.16	4.79	**11.72**	**1.60**
0.18	5.05	9.04	1.50
0.20	5.18	8.86	----

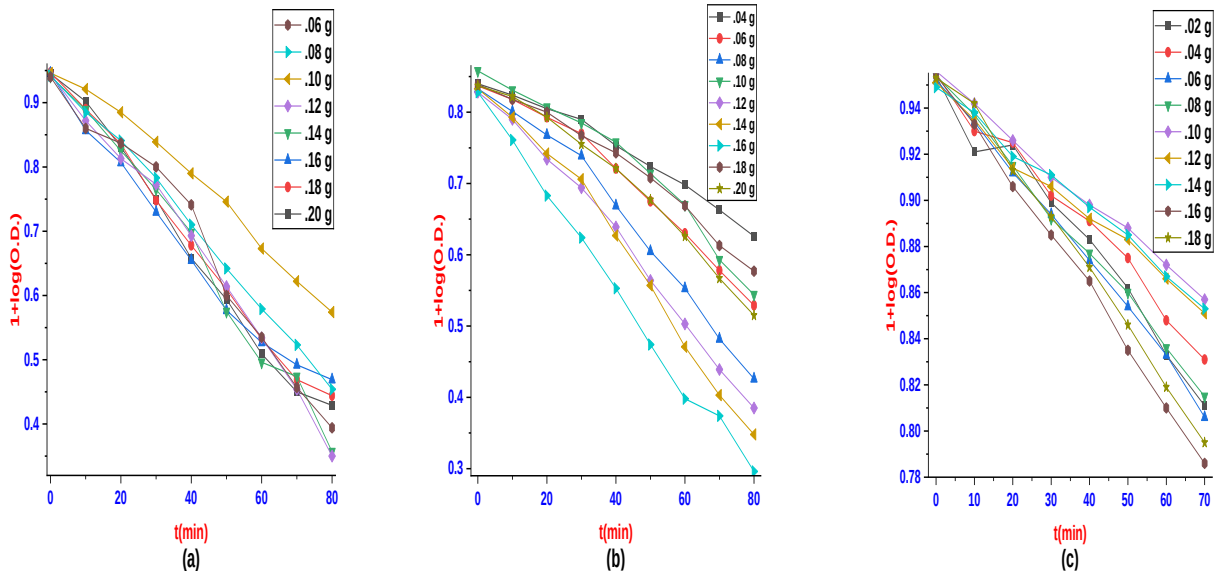

Figure 2: Effect of $BaPbCe_2O_7$ photocatalyst Dosage in g/50mL (a) AA, (b) TB (c) EB

3.4 Effect of dye concentration:

The effect of initial dye concentration on the photocatalytic degradation process for AA, TB and EB, was investigated over a concentration range of 1.0×10^{-5} to 5.6×10^{-3} Moles/Liter while keeping all other experimental parameters constant. The obtained results are presented in figure 3 and table 2. The degradation rate was found to increase with increasing dye concentration, which can be attributed to the greater availability of dye molecules to absorb incident photons and undergo excitation. However, after reaching a maximum value (at 0.4×10^{-4} M for AA, 1.0×10^{-5} M for TB, 4.8×10^{-3} M for EB), further increases in dye concentration led to a decrease in the rate of degradation. This decrease is primarily due to the excessive dye concentration intensifying the color of the solution, thereby acting as an inner filter that limits light penetration and reduces the number of photons reaching the photocatalyst surface, ultimately suppressing photocatalytic activity.

Table 2: Rate constants at different concentrations of dyes

AA		TB		EB	
Conc. of AA × 10^{-4} (moles L^{-1})	Rate constant × 10^{-4} (Sec^{-1})	Conc. of TB × 10^{-5} (moles L^{-1})	Rate constant × 10^{-4} (Sec^{-1})	Conc. of EB × 10^{-3} (moles L^{-1})	Rate constant × 10^{-4} (Sec^{-1})
0.2	4.34	**1.0**	**11.72**	4.0	1.16
0.4	**5.96**	1.2	11.08	4.2	1.21
0.6	2.47	1.4	10.98	4.4	0.70
0.8	5.53	1.6	4.59	4.6	0.90
1.0	3.86	1.8	3.90	**4.8**	**1.60**
1.2	5.67	2.0	4.93	5.0	0.74
1.4	5.46	2.2	5.97	5.2	0.91
1.6	5.67	2.4	-------	5.4	0.81
1.8	------	2.6	-------	5.6	0.72

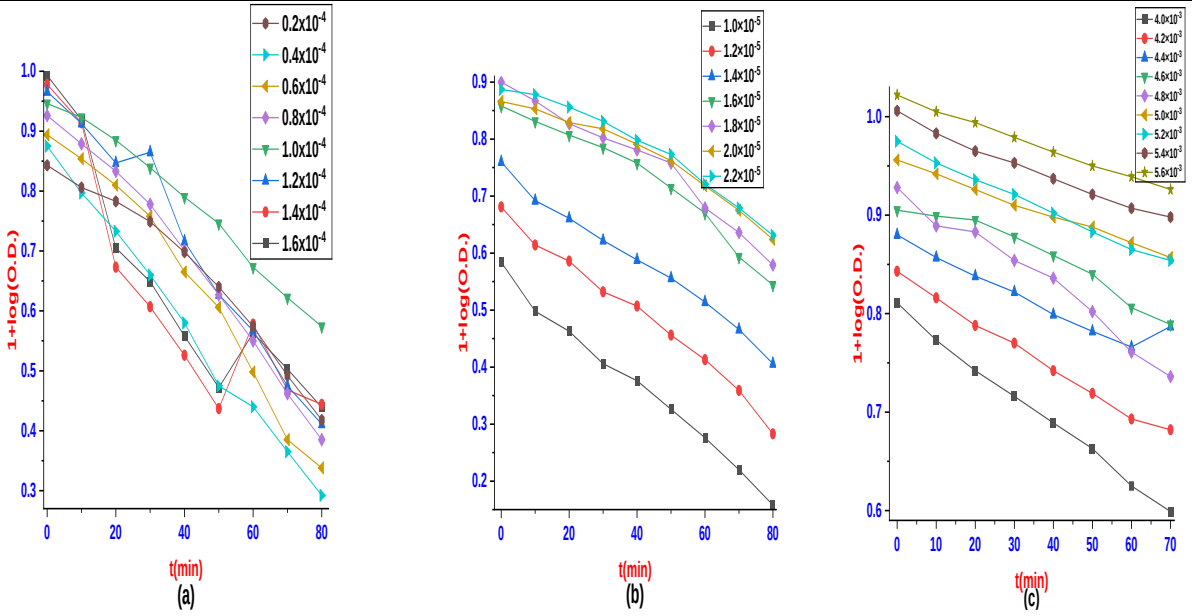

Figure 3: Effect of concentration of dyes in Moles $Litre^{-1}$ (a) AA (b) TB (c) EB

3.5 Effect of intensity of light:

The influence of light intensity on the photocatalytic degradation process was examined by varying the irradiation intensity from 930 to 1960 $mWcm^{-2}$, while maintaining all other experimental parameters constant, for all the three dyes. The corresponding results are illustrated in figure 4 and summarized in table 3. An increase in the degradation rate was observed with increasing light intensity, which can be attributed to the higher photon flux incident on the photocatalyst surface, leading to enhanced excitation of dye molecules and increased generation of electron–hole pairs. Maximum degradation rates for AA and TB dyes were achieved at a light intensity of 1960 mW cm^{-2} whereas for EB dye was achieved at 1710 $mWcm^{-2}$. However, further increases in light intensity resulted

in a decline in photocatalytic efficiency. This decrease is primarily associated with the enhanced recombination of photogenerated electron–hole pairs at higher irradiation intensities, which reduces the availability of reactive species responsible for dye degradation and consequently lowers the overall photocatalytic performance**.** Thermal side reactions are also considered as the rate reducing factor.

Table 3: Rate constants at different intensities of light

Intensity of light ($mWcm^{-2}$)	AA Rate constant × 10^{-4} (Sec^{-1})	TB Rate constant × 10^{-4} (Sec^{-1})	EB Rate constant × 10^{-4} (Sec^{-1})
930	1.22	1.96	0.36
1150	1.66	3.16	0.41
1390	2.33	4.32	0.67
1560	2.74	4.82	0.86
1710	3.29	8.62	**1.60**
1960	**5.96**	**11.72**	1.48

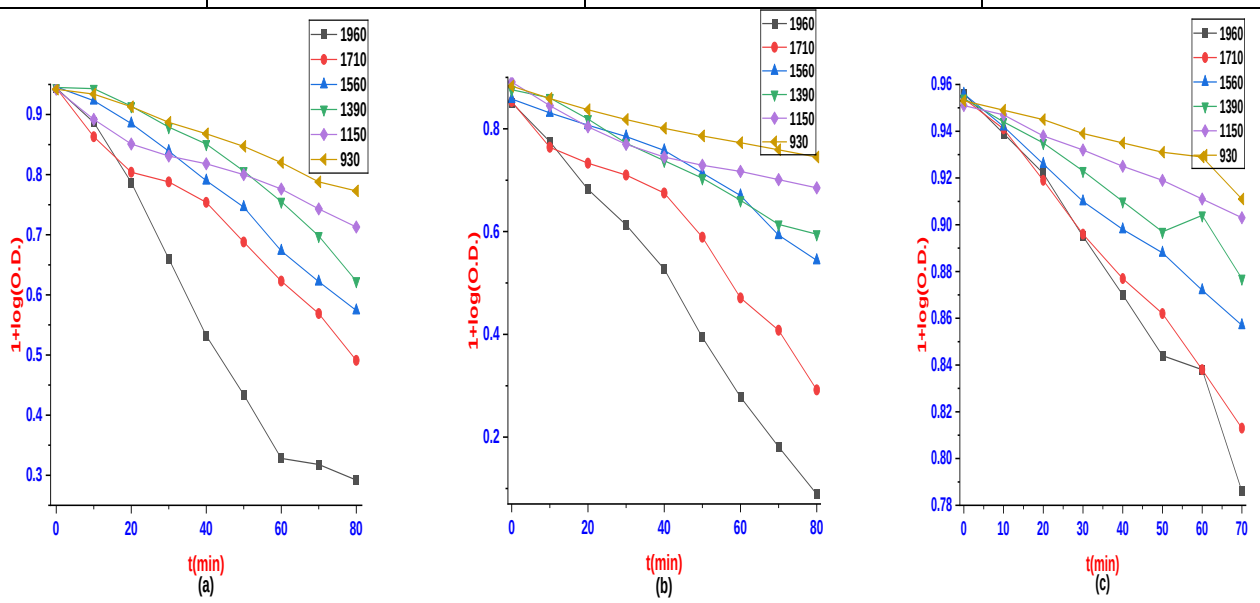

Figure 4: Effect of intensities of light (a) AA (b) TB (c) EB

3.6 Effect of pH:

The photocatalytic degradation rate of dyes is strongly influenced by the pH of the solution, as many dyes are highly pH-sensitive and may undergo structural or color changes under varying pH conditions. To evaluate this effect, the solution pH was systematically varied while keeping all other experimental parameters constant. Changes in pH were accompanied by noticeable variations in the initial optical density of the dye solutions, as reflected in the corresponding plots. The effect of pH was investigated over the range of 5.5 to 10.0 for AA, TB and EB dyes. The resulting degradation profiles are presented in figures 5(a), (b) and (c), and the corresponding rate constants are summarized in table 4. The results demonstrate that pH plays a critical role in controlling the photocatalytic degradation process. An increase in degradation rate with increasing pH was observed for TB, whereas higher degradation efficiencies for AA, TB and EB dyes were noted under acidic and basic conditions. For dyes, the maximum degradation rates were achieved at pH 10.0 for AA and EB whereas 9.1 for TB dye, highlighting the importance of pH optimization for effective dye removal.

Table 4: Rate constants at different pH

pH	AA Rate constant × 10^{-4} (Sec^{-1})	pH	TB Rate constant × 10^{-4} (Sec^{-1})	pH	EB Rate constant × 10^{-4} (Sec^{-1})
5.5	-----	7.0	3.99	5.5	1.39
6.0	-----	7.3	4.16	6.0	0.74
6.5	0.19	7.6	4.35	6.5	1.26
7.0	0.26	7.9	4.82	7.0	1.27
7.5	0.73	8.2	7.15	7.5	1.13
8.0	3.40	8.5	7.62	8.0	1.18
8.5	3.06	8.8	8.54	8.5	1.38
9.0	4.64	**9.1**	**11.72**	9.0	1.34
9.5	5.83	9.4	8.61	9.5	1.44
10.0	**5.96**	----	------	**10.0**	**1.60**

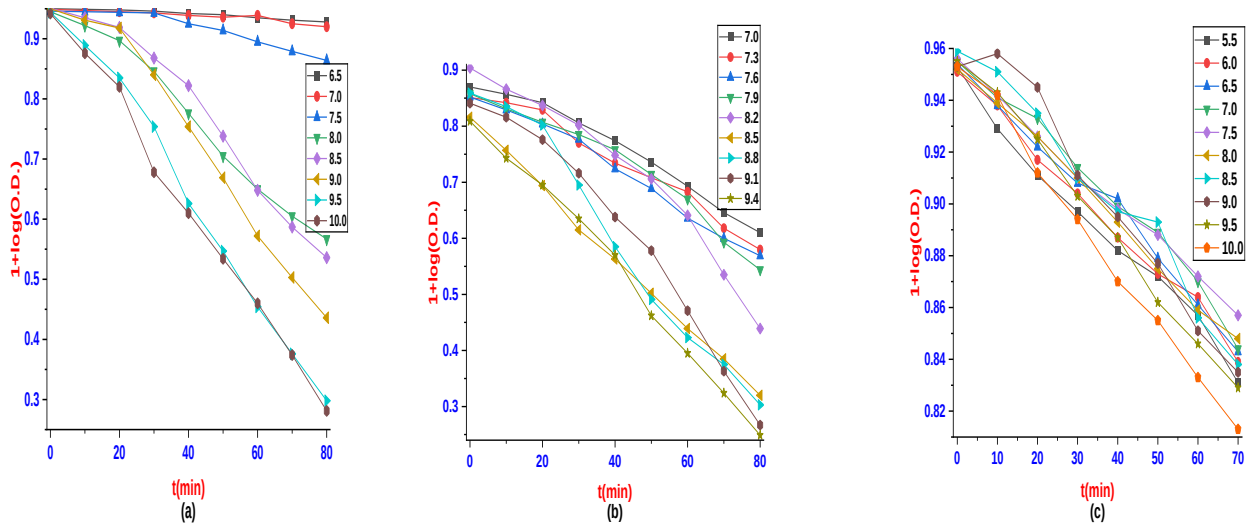

Figure 5: Effect of pH (a) AA (b) TB (c) EB

3.7 Ascertaining the reactive species:

To identify the dominant reactive species involved in the photocatalytic degradation process, scavenger experiments were carried out using various quenching agents. The degradation behavior of AA, TB and EB dyes over the $BaPbCe_2O_7$ photocatalyst was investigated in the presence of 5 mL of each scavenger and the results are presented in figure 6(a), (b) and (c) respectively. Isopropanol (IPA) acted as an effective scavenger for the AA dye, indicating that hydroxyl radicals ($^{\bullet}OH$) play a dominant role in its degradation. In contrast, EDTA significantly suppressed the degradation of TB and EB dyes, suggesting that photogenerated holes (h^+) are the primary reactive species responsible for their photocatalytic degradation. In the presence of these scavengers, the

degradation efficiency decreased markedly, stabilizing at approximately 5–7%, confirming the crucial involvement of these reactive species in the degradation mechanism [22].

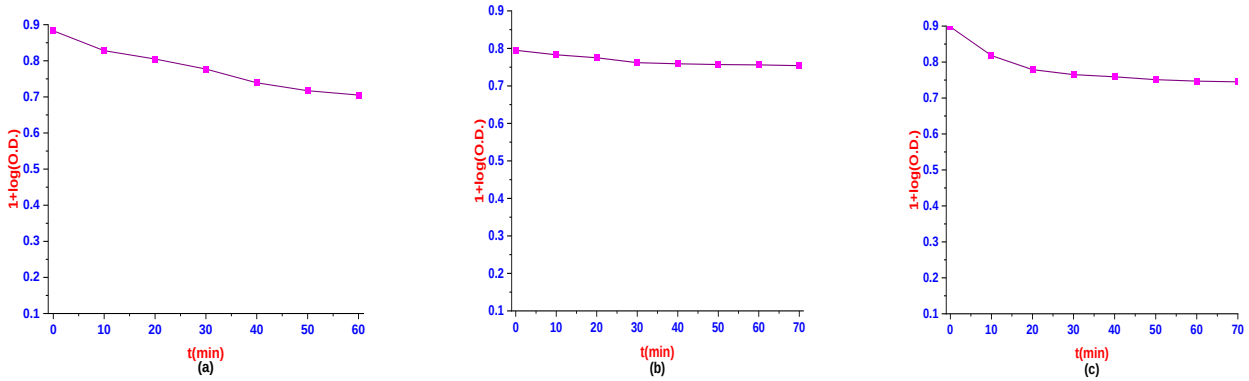

Figure 6: Scavenger study (a) AA with IPA (b) TB with EDTA (c) EB with EDTA

3.8 A comparative analysis

A comparative study is carried out for all the three dyes for their degradation and the observations state that AA, TB and EB dyes gets degraded faster with base suggesting the participation of $OH^{\bullet}$ free radical as active species causing the degradation. The same is endorsed by scavenger study where addition of IPA and EDTA (a hydroxyl free radical scavenger) ceases the reaction completely. The data with maximum conditions are given in table 5.

Table 5: A comparative data analysis for dyes

S. No.	Resulting factors	AA	TB	EB
1	λ_{max} (nm)	623	626	526
2	Conc. of Dye (moles L^{-1})	1.0×10^{-5}	0.4×10^{-4}	4.8×10^{-3}
3	pH	10.0	9.1	10.0
4	Amount of Nanoparticles (g/50 mL)	0.12	0.16	0.16
5	Intensity of Light ($mWcm^{-2}$)	1960	1960	1710
6	Degradation Time (min.)	40	18	70
7	% degradation	87%	98%	79%
8	Rate constant (Sec^{-1})	5.96×10^{-4}	11.72×10^{-4}	1.60×10^{-4}

3.9 Recycling of the photocatalyst

The recovered photocatalyst was thoroughly washed, re-calcined, and reused in successive dye degradation cycles. Notably, the photocatalytic efficiency remained nearly unchanged even after five consecutive cycles, demonstrating excellent stability and reusability. This high recyclability underscores the strong potential of the photocatalyst for practical environmental remediation applications.

3.10 Mechanism

Drawing conclusion from the results, a mechanism is proposed here in:

$_1Dye^0 + h\upsilon \rightarrow {}_1Dye^1$ (Excitation from ground state)

$_1Dye^1 + h\upsilon \rightarrow {}_1Dye^3$ (ISC to triplet state)

$BaPbCe_2O_7 + h\upsilon \rightarrow BaPbCe_2O_7$ [e^- (CB) + h^+ (VB)]

$e^- + O_2 \rightarrow O_2^{\bullet -}$ (Superoxide anion radical)

$h^+ + OH^-/H_2O \rightarrow OH^\bullet + H^+$ (Hydroxyl radical)

AA, TB, EB + $OH^\bullet \rightarrow NO_2, CO_2, H_2O$ etc.

Upon light irradiation, dye molecules in their ground state absorb photons and are excited to the singlet state, followed by intersystem crossing to the triplet state. Concurrently, the photocatalyst absorbs photons of sufficient energy to promote electrons from the valence band to the conduction band, generating photogenerated electron–hole pairs. The holes in the valence band drive oxidation reactions, while the conduction band electrons participate in reduction processes, leading to the formation of highly reactive radicals ($O_2^{\bullet -}$, $OH^\bullet$). These radicals attack the weaker bonds of the dye molecules, resulting in their fragmentation into smaller, environmentally benign end products such as CO_2, H_2O and NO_2. This mechanism highlights the efficiency and environmental compatibility of the photocatalytic degradation process.

IV. Conclusion:

$BaPbCe_2O_7$ nanoparticles were successfully synthesized using the co-precipitation method, achieving a yield of 73% after calcination. The nanoparticles, with an average crystallite size of 58.12 nm, demonstrated remarkable photocatalytic activity in the degradation of Azure A, Toluidine blue and Erythrosine B dyes in aqueous solutions. The photodegradation efficiency increased with catalyst dosage up to an optimal level, beyond which it reached a plateau. Additionally, the degradation rate was significantly affected by factors such as initial dye concentration, doses of photocatalyst, pH and light intensity. Enhanced photodegradation was observed at lower dye concentrations, higher pH values, and increased light intensities, underscoring the potential of the synthesized $BaPbCe_2O_7$ nanoparticles as an effective and versatile photocatalyst for environmental remediation.

V. Acknowledgement: The authors are thankful to the Materials Research Centre, MNIT Jaipur, Rajasthan, India, SAIF laboratory, Punjab University, Chandigarh, India for carrying out the analysis.

REFERENCES

1. Sharma, S., Chaplot, L.J., Kumawat, S.A., Intodia, K. Photocatalytic degradation of Azure-A using visible light-responsive metal bismuth iodides: A Comparative study. *Oriental J. Chem.*, **2024**, 40, 1027-1034.
2. Epstein, J.B., Scully, C., Spinelli, J. Toluidine blue and Lugol's iodine application in the assessment of oral malignant disease and lesions at risk of malignancy. *J. Oral Pathol. Med*., **1992**, 21,160–163.
3. Epstein, J.B., Oakley, C., Millner, A., Emerton, S., vander, M. E., Le, N. The utility of toluidine blue application as a diagnostic aid in patients previously treated for upper oropharyngeal carcinoma. *Oral Surg. Oral Med. Oral Pathol. Oral Radiol. Endod.*, **1997**,83,537–547.
4. Gandalfo, S., Pentenero, M., Broccoletti, R., Pagano, M., Carrozzo, M., Scully, C. Toluidine blue uptake in potentially malignant lesions in vivo: Clinical and histological assessment. *Oral Oncol.*, **2006**,42,89–95.
5. Basavaraju, B.C., Chandrashekara, M.B., Mantelingu, K., Harsha, M., Kumara, N.M. Degradation of a xanthene dye Erythrosine B by Chloramine-T in acid medium: A Spectrophotometric Approach. *Int. J. Creat. Res. Thoug.*, **2018**, 6 (2), 830-841.

6. Kumar, A., Pandey, G., A review on the factors affecting the photocatalytic degradation of hazardous materials, *Mater. Sci. Eng. Int. J.*, **2017**, 1(3), 1-10.
7. Al-Nuaim, M. A., Alwasiti, A. A., Shnain, Z. Y., The photocatalytic process in the treatment of polluted water, *Chem. Papers*, **2023**, 77(2), 677-701.
8. Linic, S., Aslam, U., Boerigter, C., Morabito. M. Photochemical transformations on plasmonic metal nanoparticles. *Nat. Mat.*, **2015**, 14, 567-576.
9. Muthuvel, A., Jothibas, M., Manoharan. C. Synthesis of copper oxide nanoparticles by chemical and biogenic methods: photocatalytic degradation and in vitro antioxidant activity. *Nanotech. Environ. Eng.*, **2020**, 5,14.
10. Alarifi, S., Ali, D., Al-Bishri. W. In vitro apoptotic and DNA damaging potential of nanobarium oxide. *Int. J. Nanomed.*, **2016**, 11, 249-257.
11. Renukadevi, R., Sundaram, R., Kaviyarasu. K. Barium Oxide nanoparticles with Robust Catalytic, Photocatalytic and Humidity Sensing Properties. *J. Nanostr.*, **2020**, 10, 167-176.
12. E. Sundharam, A. Kingson, S. Jeevanraj, C. Chinnusamy. Effect of Ultrasonication on the Synthesis of Barium Oxide Nanoparticles. *J. Bionanosci.*, **2017**, 11, 310-314.
13. Choudhary, R. V., Jha, V., Jana. P. Epoxidation of styrene by TBHP to styrene oxide using barium oxide as a highly active/selective and reusable solid catalyst. *Green Chem.*, **2006**, 8 (8), 689-690,
14. Hamid, A., Khan, M., Hayat, A. et al., Probing the physio-chemical appraisal of green synthesized PbO nanoparticles in PbO-PVC nanocomposite polymer membranes, *Spectrochimica Acta Part A: Mol. Biomol. Spect.*, **2020**, 235, 118303.
15. Sonmez, M.S., Kumar, R.V., Leaching of waste battery paste components. Part 1: Lead citrate synthesis from PbO and PbO_2, *Hydrometallurgy*, **2009**, 95, 53-60.
16. Sljuki, B., Banks, C.E., Crossley. A., Richard, G., Compton, R.G., Lead (IV) oxide–graphite composite electrodes: Application to sensing of ammonia, nitrite and phenols, *Analyt. Chimica Acta*, **2007**, 587, 240–246.
17. Sharma, D., Mehta, B.R. Nanostructured TiO_2 thin films sensitized by CeO_2 as an inexpensive photoanode for enhanced photoactivity of water oxidation. *J. Alloys Compd.* **2018**, 749, 329–335.
18. Prajapati, K.D., Chouhan, K.J., Menaria, J., Tanwer, S.T., Bhardwaj, S. Fabrication and Characterization of Photocatalyst Pb_3CdO_7 for Degradation of Azure- A. *J. Environ. Sci. Pollut. Res.* **2024**, 10, 485–491.
19. Aboutaleb, W.A., El-Salamony, R.A. Effect of Fe_2O_3-CeO_2 nanocomposite synthesis method on the Congo red dye photodegradation under visible light irradiation. *Mater. Chem. Phys.* **2019**, 236, 121724.
20. Wang, B., Zhu, B., Yun, S., Zhang, W., Xia, C., Afzal, M., Cai, Y., Liu, Y., Wang, Y., Wang, H. Fast ionic conduction in semiconductor $CeO_{2-\delta}$ electrolyte fuel cells. *NPG Asia Mater.* **2019**, 11, 51-59.
21. Tanwer, S.T., Menaria, J., Prajapati, K.D., Chouhan, K.J., Bhardwaj, S. Optoelectronic properties of fabricated $BaPbCe_2O_7$ nanoparticles for photocatalytic breakdown of malachite green: a greener approach. *Int. J. Creat. Res. Thoug.*, **2025**, 13, 2320-2882.
22. Das, A., Adak, K.M. Kinetic and mechanistic way for photocatalytic degradation of pollutants from textile wastewater by graphene oxide supported nanocomposite. *Next Mat. Elesvier*, **2024**, 3, 100153.